A topological approach to characterising optical skyrmions

Amy McWilliam[a], Claire M. Cisowski[a], Zhujun Ye[a], Fiona C. Speirits[a], Jörg B. Götte[a], Stephen M. Barnett[a], and Sonja Franke-Arnold[a]

[a]School of Physics and Astronomy, University of Glasgow, Glasgow, G12 8QQ, UK

ABSTRACT

Skyrmions are topologically protected field configurations characterised by a topological index, the skyrmion number. Optical skyrmions are ideally suited to investigate topological structures due to the ease of generating arbitrary light fields, and the freedom from energy constraints encountered by, for example, magnetic skyrmions. Building on our previous work of a topologically defined skyrmion number,[1] here we demonstrate the conservation of the skyrmion number of hedgehog skyrmions and bimerons under propagation. We furthermore generate tunable multi-skyrmions from superpositions of oppositely polarised Gaussian and split-vortex beams of different waists, and find that the skyrmion number is conserved as a function of waist scaling. For both cases, the topological definition of the skyrmion number forms an intuitive geometric approach to understanding the underlying topology and to identifying the individual skyrmion structures.

Keywords: Skyrmions, optical skyrmions, topology, structured light, vector beams, orbital angular momentum

1. INTRODUCTION

Skyrmions have been an area of interest since the idea of using a topological model to describe the excitations in the non-linear field of the nucleon was first postulated by Tony Skyrme in 1961.[2] Although Skyrme's ideas were never adopted for their intended purpose of describing sub-atomic particles, these topological quasi particles have since been studied in many areas of physics, including the study of mesons and baryons, quantum liquids,[3] spintronics,[4] string theory,[5] Bose-condensates and atoms,[6,7] and perhaps most notably, in magnetic materials.[8–10] More recently, the optical analogue to skyrmions has become of interest where they have been observed in evanescent fields[11] and paraxial beams.[12–14]

The development of tools such as digital micromirror devices, spatial light modulators and q-plates over recent decades have allowed the easy generation of structured light beams. By controlling the amplitude, phase and polarisation of the propagating light field, complex structures can be created at will. Some important examples of these include beams carrying orbital angular momentum (OAM), vector-vortex beams and Poincaré beams,[15–17] all of which contain interesting topological features, such as phase and polarisation singularities. Beams with spatially varying polarisation distributions have also been shown to have skyrmionic structures embedded within their polarisation profiles.[12–14]

As skyrmionic structures are found within polarisation profiles, it is simple to experimentally identify them by measuring the spatially varying Stokes parameters $\mathbf{S}(x, y)$, over the entire transverse plane, which map polarisation states onto the Poincaré sphere. Although the polarisation profiles of structured paraxial beams can take many forms, the topology can be characterised by a single topological quantum number, the Skyrmion number, n, which is a property of the underlying skyrmion field and counts the number of complete wrappings of $\mathbf{S}$ around the Poincaré sphere. For a beam to be considered an optical skyrmion, it would usually include every possible polarisation state at least once in its transverse plane with their distribution obeying a set of topological rules.[18] There do exist, however, fractional or non-integer skyrmion beams that do not have this property, but nonetheless, still contain skyrmionic structures.[19]

Further author information: (Send correspondence to A.M.)
A.M.: E-mail: a.mcwilliam.1@research.gla.ac.uk,
S.F-.A.: E-mail: Sonja.Franke-Arnold@glasgow.ac.uk,

The skyrmion number is a global property of a light beam that relies on polarisation gradients (as shown later in Eq. 1). Previous work has relied on using this definition of n to evaluate skyrmion numbers,[12,20,21] however, a property of derivatives is their inherent sensitivity to noise, making experimental evaluation challenging. We have recently derived an alternative definition for the skyrmion number based on polarisation singularities and associated winding numbers and demonstrated that this definition provides a robust and accurate way to determine skyrmion numbers from experimental data.[1] Additionally, the proposed method provides an intuitive geometric insight into skyrmionic structures allowing further understanding of their underlying topology.

Here, we will give a brief description of this topological approach to finding the skyrmion number, and expand on the experimental work outlined in Ref. 1, by looking at the experimental propagation of paraxial optical skyrmions. Additionally, we will present an alternative way to generate optical skyrmions using OAM beams with split vortices.[22–24] These beams provide an additional freedom in the polarisation texture of the skyrmion, by control of the location of the polarisation singulatities, and are reminiscent of the multi-skyrmions that have been created using rational maps.[18]

2. TOPOLOGICAL DEFINITION OF THE SKYRMION NUMBER

For a beam propagating in the z direction, n is given by the expression,

$$n = \frac{1}{4\pi}\int_A \mathbf{\Sigma}\cdot \mathrm{d}\mathbf{A} = \frac{1}{4\pi}\int_A \mathbf{S}_R \cdot \left(\frac{\partial \mathbf{S}_R}{\partial x}\times\frac{\partial \mathbf{S}_R}{\partial y}\right)\mathrm{d}x\mathrm{d}y, \tag{1}$$

where $\mathbf{\Sigma}$ is known as the skyrmion field. Here, $\mathbf{S}_R = R\mathbf{S} = [S_x, S_y, S_z]^T$ is a generalised Stokes vector that relates to the conventional, normalised and spatially resolved, reduced Stokes vector, $\mathbf{S} = [S_1, S_2, S_3]^T$ through an arbitrary rotation described by the matrix R. The integral in Eq. 1 runs over the surface A, which describes the entire transverse plane perpendicular to the propagation direction, therefore, making n a global property of the beam.[12]

One property of the Skyrmion field is that it is divergenceless ($\nabla\cdot\mathbf{\Sigma} = 0$). This transverse property of $\mathbf{\Sigma}$ allows it to be expressed as the curl of a vector field, $\mathbf{\Sigma} = \nabla\times\mathbf{v}$. By applying Stokes's theorem we obtain,

$$n = \frac{1}{4\pi}\int_A \mathbf{\Sigma}\cdot d\mathbf{A} = \frac{1}{4\pi}\int_A (\nabla\times\mathbf{v})\cdot d\mathbf{A} = \frac{1}{4\pi}\oint_C \mathbf{v}\cdot d\boldsymbol{l}. \tag{2}$$

Here, C is an integration path over the transverse plane, A, suitably chosen to avoid any singularities present in $\mathbf{v}$. The form of $\mathbf{v}$ is not unique, however, $\mathbf{v} = -S_z\nabla\Phi$, is a suitable choice, where Φ is often referred to as the Stokes phase and can be written as[1,19] ,

$$\Phi = \arctan(S_y/S_x). \tag{3}$$

Using this, the Skyrmion number can be expressed as a line integral that depends on the local Stokes parameter and variation of Φ around the integration path,

$$n = \frac{1}{4\pi}\oint_C S_z\nabla\Phi\cdot d\boldsymbol{l}. \tag{4}$$

The integration path, C, should enclose as much of the beam profile as possible (although, ideally the entire transverse plane), but exclude any singularities in $\mathbf{v}$, and hence Φ, as shown in Figure 1. The sections of the integration path which connect the beam periphery to the locations of the singularities cancel, which leaves us with two (or more) closed circular line integrals: One evaluated counter-clockwise at a radius $\rho\to\infty$ (α), and one or more evaluated clockwise around the singularities (β_j). This allows the integral to be simplified to,

$$n = \sum_j \frac{1}{4\pi}\oint_{\beta_j} S_z\nabla\Phi\cdot d\boldsymbol{l} - \frac{1}{4\pi}\oint_\alpha S_z\nabla\Phi\cdot d\boldsymbol{l}. \tag{5}$$

At each singularity, with position (x_j, y_j), we can simply take the local value of $S_z^{(j)}$, and as such it can be taken out of the integral. At the outside of the beam, the Stokes parameter converges to a single value, thus $\bar{S}_z^{(\infty)}$

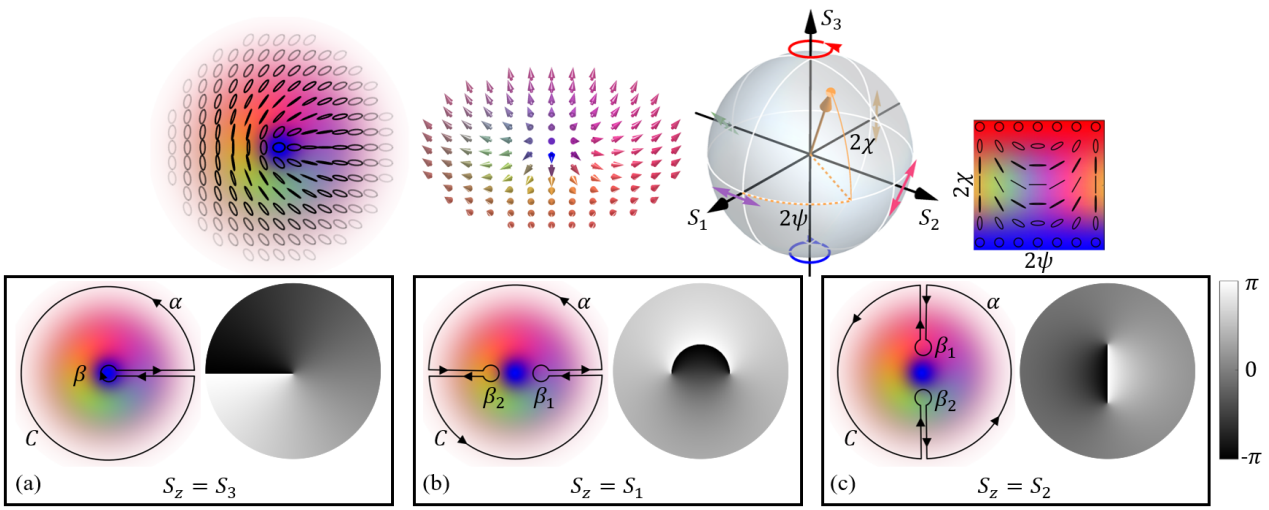

Figure 1. Illustration of the topological definition of the skyrmion number. Top row shows the polarisation profile of an $n = 1$ skyrmion beam represented as polarisation ellipses (left) and unitary Stokes vectors (centre). On the right is the Poincaré sphere with ellipticity (χ) and orientation (ψ) angles indicated. As an inset, we include the polarisation colour scheme used throughout, where we show intensity as opacity. (a), (b) and (c) show integration paths (left) and Stokes phase profiles Φ (right) when evaluated for a choice of $S_z = S_1$, S_2 and S_3.

can be found and also taken out of the integral. The remaining integrals are related to the polarisation winding number, given by $N = (2\pi)^{-1} \oint \nabla\Phi \cdot d\boldsymbol{l}$,[25] which counts the number of turns $\mathbf{S}$ completes on the Poincaré sphere when following the respective circular paths. From the definition, N, must be an integer, therefore, is free from noise. We now obtain our final topological definition for the Skyrmion number,[1,19]

$$n = \frac{1}{2}\left(\sum_j S_z^{(j)} N_j - \bar{S}_z^{(\infty)} N_\infty\right), \tag{6}$$

which depends only on the Stokes vector at the position of the singularities and at the beam periphery, and the corresponding integer winding numbers on the Poincaré sphere.

The above definition was derived in terms of a generalised Stokes vector $\mathbf{S}_R = [S_x, S_y, S_z]^T$. As the Skyrmion field, Σ, is invariant under rotations, the orientation of the Poincaré sphere is irrelevant, and any $\mathbf{S}_R$ can be chosen when calculating n.

Here, we will give examples using an $n = 1$ Skyrmion beam to illustrate how Eq. 6 links to the topology of the polarisation profile and how the choice of $\mathbf{S}_R$ can make the topological features more apparent.

In the top left of Figure 1, we show the polarisation profile of an $n = 1$ skyrmion beam, where we use the indicated colour map to represent the spatially resolved polarisation states. We also show the corresponding vectorial representation of $\mathbf{S}(x, y)$, indicating the local direction of the Stokes vector on the Poincaré sphere. Figure 1(a) displays Φ when a choice of $\mathbf{S}_R = [S_1, S_2, S_3]^T$ is made, resulting in a singularity in the centre at the left-handed circular polarisation position, and a delocalised singularity at the beam periphery. To avoid the singularity locations in this case, we use an integration path (C) as shown on the left of (a). At the central singularity location, $S_3 = -1$ and as $\rho \to \infty$, $S_3 = 1$, and the polarisation winding number, $N = -1$ in both cases, allowing Eq. 6 to be evaluated as $n = \frac{1}{2}\{(-1)(-1) - (1)(-1)\} = 1$.

Alternatively, we can choose $\mathbf{S}_R = [S_2, S_3, S_1]^T$, as illustrated in Figure 1(b). This choice results in two singularities located at the positions of the horizontal and vertical linear polarisation states. Following the same procedure as before and using the integration path as illustrated gives $n = \frac{1}{2}\{[(1)(1) + (-1)(-1)] - 0\} = 1$, resulting in the same correct skyrmion number. Here, we have used that, for this choice, $S_1 = 1$ at β_1, $S_1 = -1$ at β_2, and $N = 0$ around the beam periphery.

In Figure 1(c) we provide an illustration for a choice of $\mathbf{S}_R = [S_3, S_1, S_2]^T$, where, if the same procedure is followed and Eq. 6 evaluated, $n = 1$ will again be obtained. From these simple examples, it can be seen, that unlike Eq. 1, our topological definition of the skyrmion number does not require any derivatives or integration and instead can be read directly from inspection of the polarisation profile. In the following section, we will show experimental results of propagated skyrmion beams along with calculated skyrmion numbers and demonstrate that using the topological method, it is possible to achieve an increase in accuracy, keeping in line with the results shown in Ref. 1.

3. PROPAGATION OF PARAXIAL SKYRMIONIC BEAMS

In this section, we will describe the experimental generation and measurement of propagating optical skyrmions in order to investigate the conservation of the skyrmion number. For this, we chose to observe the beam propagation under weak focusing, still staying within the paraxial regime.

A beam with spatially varying polarisation and skyrmion number n can be generated from the superposition of orthogonally polarised Laguerre-Gaussian modes, LG_p^ℓ,[12,26]

$$|\psi_n\rangle = \frac{1}{\sqrt{2}} \left(\mathrm{LG}_0^0 |0\rangle + \mathrm{LG}_0^n |1\rangle \right), \tag{7}$$

where p and ℓ are the radial and azimuthal mode numbers, respectively. Here, $|0\rangle$ and $|1\rangle$ represent any two orthogonal polarisation states. The orthogonal polarisations used in the generation make up the Schmidt basis of the beam.

Experimentally, we generate optical Skyrmions via digital holograms by employing a digital micromirror device (DMD). A DMD can modulate any incident polarisation and therefore, gives the freedom to create beams with arbitrary polarisation structures by shaping amplitude, phase and polarisation simultaneously. The methods for this are outlined in Refs. 27,28 and the supporting information of 1. The spatially varying Stokes parameters are measured using a rotating waveplate setup[1,27] allowing the transverse polarisation profiles to be realised (see Figure 2).

To view the propagation of the generated beams with focusing, we use a 150 mm lens and a camera mounted on a motorised translation stage, allowing precise measurement of the transverse polarisation at different propagation planes. We choose to generate beams using either a circular ($|0\rangle = |l\rangle$, $|1\rangle = |r\rangle$) or linear ($|0\rangle = |h\rangle$, $|1\rangle = |v\rangle$) polarisation basis, resulting in polarisation textures with either a skyrmionic or a bimeronic structure.[29]

In Figure 2(a), we show experimentally measured polarisation profiles of the focusing of an $n = 1$ skyrmion beam at different transverse planes after the 150 mm lens, and in Figure 2(b) we show the equivalent measurements for an $n = 1$ bimeron. At a propagation distance of $z = 0$ cm, we have the original skyrmion beam and at 15 cm ($z = f$), we have the polarisation profile at the focus. In Figure 2, we have cropped the experimental images to different beam waist multiples, as indicated, to reflect the change in beam size with focusing, allowing the polarisation to be resolved clearly. The continuous rotation seen in the polarisation profiles as the beam propagates can be explained by the different relative Gouy phase between the constituent modes used to construct the beam. The entire profile rotates by $\left|\frac{\pi}{2}\right|$ as it propagates from the far field to the focus, with the majority of the rotation happening close to the focal point, within about two Rayleigh ranges (z_R). This is, of course, due to the dependence of the Gouy phase on $\tan^{-1}(z/z_R)$.[26] However, despite the visual change in the polarisation pattern, the skyrmion number should remain unchanged. Interestingly, it is possible to trace out lines of constant polarisation, as shown in Figure 2(c), and it has recently been demonstrated[30] that these are equivalent to skyrmion field lines (Σ).

To show the invariance of the skyrmion number, we evaluate n using the spatially resolved Stokes parameters and both Eq. 1 and our topological method (Eq. 6), and summarise the results in Table 1. For both methods, we subtract the background noise, low pass Fourier filter the camera images to remove any unwanted diffraction artefacts and crop the images to a disk, outside of which, the intensity is $\leq 5\%$ of the peak intensity. For Eq. 1, the surface integral was performed over the entire grid space in order to find the skyrmion number. For Eq. 6 we choose to perform the evaluation by assigning either $S_z = S_3$ or $S_z = S_1$.

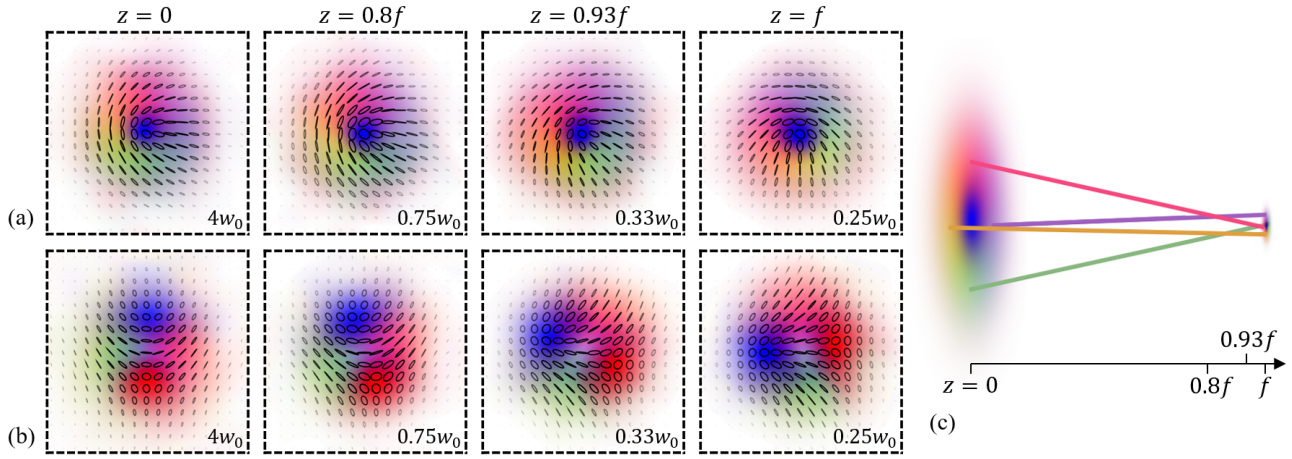

Figure 2. Experimentally measured transverse polarisation profiles of focusing using a 150 mm lens. (a) An $n = 1$ optical skyrmion generated using Eq. 7 and a circular polarisation basis ($|0\rangle = |l\rangle$, $|1\rangle = |r\rangle$). (b) An $n = 1$ bimeron generated using a linear polarisation basis ($|0\rangle = |h\rangle$, $|1\rangle = |v\rangle$). The propagation distance after the lens is indicated on the top row as a fraction of focal length (f) and the numbers on the bottom right of each beam represent the the real width and height of the images as a multiple of the original beam waist. (c) Trace of the lines of constant polarisation for the focusing skyrmion beam given in (a).

For both methods, we achieve skyrmion numbers close to 1 for every propagation distance, demonstrating the invariance of the skyrmion number under paraxial propagation. In all cases, the highest accuracy in the skyrmion number was attained when using Eq. 6 and evaluating using a mutually unbiased basis to the Schmidt basis used to define the beam in Eq. 7 (i.e. assigning $S_z = S_1$ for the skyrmion shown in Figure 2(a) and $S_z = S_3$ for the bimeron shown in Figure 2(b)).

The reason for this improved accuracy lies in the fact that we have moved the relevant path integrals away from beam areas with low intensity which are dominated by noise. The better performance of the topological approach in the presence of noise has been further confirmed by applying background noise to simulated data. The results and full details of this can be seen in Ref. 1.

Table 1. Comparison of experimentally measured skyrmion numbers at different propagation distances for the $n = 1$ skyrmion and bimeron shown in Figure 2 and evaluated using Eqs. 1 and 6.

Type	Method	Propagation distance			
		0	$0.8f$	$0.93f$	f
skyrmion	Eq. 1	0.915	0.942	0.930	0.929
	Eq. 6 ($S_z = S_3$)	0.914	0.946	0.947	0.943
	Eq. 6 ($S_z = S_1$)	0.999	0.998	0.988	0.998
bimeron	Eq. 1	0.922	0.931	0.921	0.905
	Eq. 6 ($S_z = S_1$)	0.955	0.964	0.960	0.949
	Eq. 6 ($S_z = S_3$)	0.999	0.985	0.971	0.995

4. GENERATION OF TUNABLE OPTICAL MULTI-SKYRMIONS

Typically, optical skyrmions are generated such that the centre and periphery of their transverse polarisation distributions have orthogonal polarisations, with all other polarisation states appearing in a winding arrangement in the regions in between. This is the case for the examples shown here so far (see Figure 2), and for the optical skyrmions investigated in other work.[13,14,21,31,32] The reason for this is, perhaps, due to the resemblance of the skyrmion field of beams of this form and that seen in the more familiar magnetic skyrmions. Magnetic skyrmions

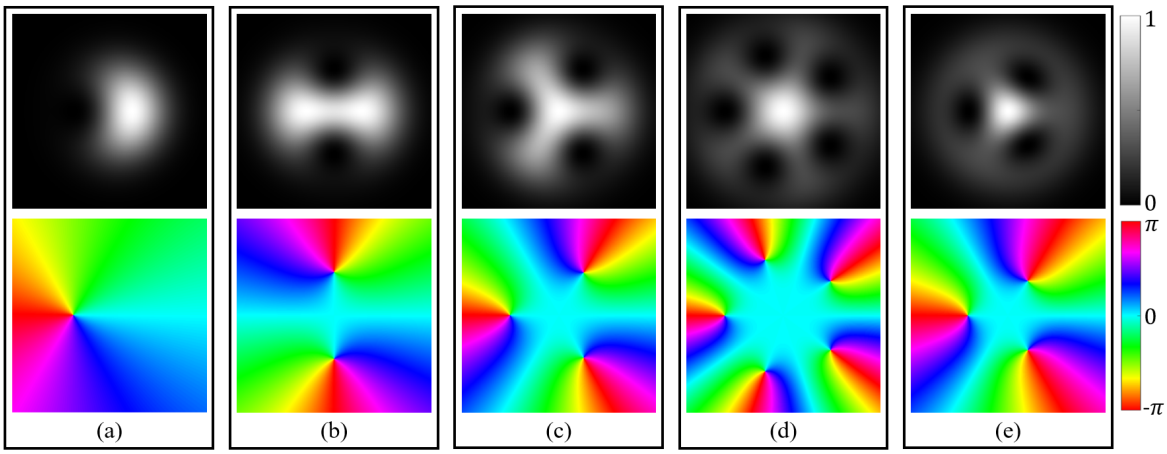

Figure 3. Intensity (top row) and electric field phase distributions (bottom row) of equal superpositions of LG_0^ℓ modes and a Gaussian. (a-d) show the superposition of an LG_0^1, LG_0^2, LG_0^3 and LG_0^5 with a Gaussian of equal waist w_0, respectively, whereas in (e) an LG_0^3 mode is superimposed with a Gaussian with a beam waist of $0.7w_0$. The intensity and phase maps used are shown on the right.

are subject to certain physical constraints (for example energy minimisation and conservation laws), resulting in configurations in magnetic films where the spins are all aligned orthonormal to the plane of the film, with the exception of a specific, finite region in which the spins progressively rotate. Energy minimisation then leads to structures with circular symmetry.[8] However, unlike magnetic skyrmions, paraxial beams are limited only by Maxwell's equations. Therefore, in principle, it is possible to generate arbitrary polarisation patterns, allowing the field of free space optics to be used to investigate interesting topological structures.

Here, we will give examples of optical skyrmions generated using split-vortex beams and show how the skyrmion number and its topology is related to the OAM of the constituent beam. It is known that the coherent mixture of an LG_0^1 mode with a Gaussian beam can displace the location of the phase vortex singularity from the centre of the beam,[22,23] as is shown in Figure 3(a). Due to the non rotationally symmetric intensity distributions of these beams, they have been used to observe the mechanical rotational motion of beams carrying OAM about their propagation axis.[22] However, from the addition of a Gaussian beam to LG modes with higher OAM values, we have the effect of vortex splitting where an LG beam with a single central vortex of order ℓ will now have $|\ell|$ vortices of order 1 (or -1), as shown in Figure 3(b-d) for $\mathrm{LG}_0^{2,3,5}$+ Gaussian beams. Additionally, as shown by the example in Figure 3(e), by changing the ratio between the beam waists of the two superimposed beams, we can control the vortex singularity positions in reference to the beam centre.

It is possible to generate optical skyrmions using these split vortex beams and a similar recipe as before. Figure 4 shows simulated polarisation profiles of beams of the form,

$$|\psi\rangle = \mathrm{LG}_0^0(w_0)\,|l\rangle + \left(\mathrm{LG}_0^\ell(w_0) + \mathrm{LG}_0^0(\delta w_0)\right)|r\rangle\,, \tag{8}$$

where δ is the ratio between the beam waist of the additional Gaussian beam used to create the split vortex beam and the other LG modes which have the same waist w_0. This provides control over the position of the polarisation singularities.

In Figure 4(a) we show an example of a beam with $n = 2$, the polarisation profile of which is reminiscent of the multi-skyrmions created using rational maps as seen in Ref. 18. Additionally, we show the associated Stokes phase profiles for interpretation in different polarisation bases by assigning $S_z = S_1$, S_2 or S_3. From inspection of the polarisation and comparing it to Figure 1, we can see that it appears similar to two partially overlapping $n = 1$ skyrmions, and indeed, when calculating the skyrmion number of this beam using our topological method (Eq. 6) and $S_z = S_3$, Φ contains two singularities located at the left handed circular polarisation locations. Both of these areas contribute a value of $1/2$ to the overall skyrmion number and the outside contributes a value of 1. This shows how the topological approach to finding n can allow multi-skyrmions to be interpreted as a combination of individual skyrmion structures (as also demonstrated in Ref. 1 for the example of a multi-skyrmion ring).

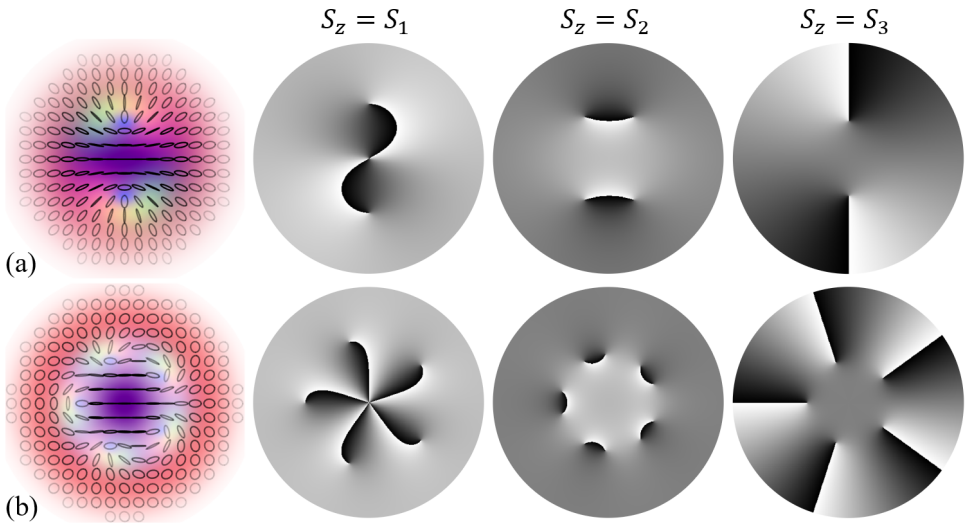

Figure 4. Simulated polarisation profiles and Stokes phase (Φ) distributions of optical skyrmions generated using split vortex beams as described by Eq. 8. The left of (a) shows an $n = 2$ skyrmion created using $\ell = 2$ and $\delta = 0.7$ in Eq. 8 and (b) shows an $n = 5$ skyrmion created using $\ell = 5$ and $\delta = 0.7$. On the right of (a) and (b), the relevant Φ is displayed when interpreting the skyrmion in different polarisation bases by assigning $S_z = S_1,\ S_2,\ S_3$, as indicated.

Figure 4(b) shows a similar example but for a beam with $n = 5$.

As mentioned above, changing the ratio between the beam waists of the LG and Gaussian mode in a split vortex beam will change the distance of the vortex singularities from the beam centre. In Figure 5, we show the effect of changing this ratio δ on the resulting polarisation distributions and the singularities in Φ for a beam of the form of Eq. 8 with $\ell = 3$. On the bottom row of Figure 5 we show Φ profiles when setting $S_z = S_3$, from which it can be seen that the singularities in Φ move further from the beam centre, along with the pure left-handed circular polarisation components, as δ increases from 0 to 1. In fact, the location of these singularities is, perhaps as expected, the same as the location of the phase singularities in the split vortex beam, displaying the link between skyrmionic structures and the underlying differential OAM of the contributing modes.[12] Despite the difference in appearance of the polarisation patterns, all of the beams shown in Figure 5 have the same skyrmion number of $n = 3$.

Beams of the form of those shown in Figures 4 and 5 and described by Eq. 8 give a further example of beams that can be added to the growing field of paraxial optical skyrmions and provides an example of ways in which optics can be used to investigate topologies not permitted in other fields.

5. CONCLUSION

We have summarised a previously introduced topological approach for characterising optical skyrmions solely via their polarisation singularities and associated winding numbers. This method has been shown to not only provide increased accuracy and better performance in the presence of noise, but also provides an intuitive geometric insight into the underlying skyrmionic structures. Here, we have built on the previous work by presenting the results of experimentally measured optical skyrmions under weak focusing, demonstrating that the topological approach also provides advantages when considering propagation. Additionally, we have introduced a new way of generating optical multi-skyrmions with tunable polarisation textures using split-vortex beams, showing how the topological approach to finding n allows the individual skyrmion structures to be easily identified. Research within the field of optical skyrmions is still in its infancy, and we believe that the tunable multi-skyrmions presented here could be an interesting addition to the growing research field.

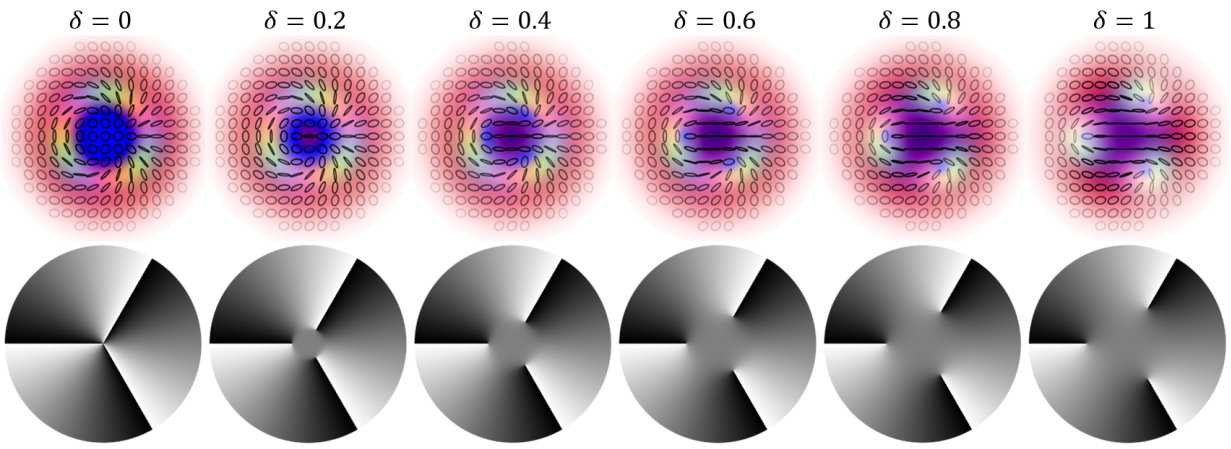

Figure 5. Simulated $n = 3$ optical skyrmions of the form of Eq. 8 for $\ell = 3$ and varying δ. The top row shows the polarisation profiles and the bottom row the Φ profiles when $S_z = S_3$ is chosen.

ACKNOWLEDGMENTS

A.M. acknowledges financial support from the UK Research and Innovation Council via grant EPSRC/DTP 2020/21/EP/T517896/1. C.M.C., S.M. B and S.F.-A. acknowledge financial support from the Royal Society through a Newton International fellowship NIF/R1/192384 and a Research Professorship RP150122. J.B.G acknowledges financial support from the EPSRC via grant EP/V048449/1 and the Leverhulme Trust.

REFERENCES

[1] McWilliam, A., Cisowski, C. M., Ye, Z., Speirits, F. C., Götte, J. B., Barnett, S. M., and Franke-Arnold, S., "Topological approach of characterizing optical skyrmions and multi-skyrmions," *Laser & Photonics Reviews* **17**(9), 2300155 (2023).

[2] Skyrme, T. H. R. and Schonland, B. F. J., "A non-linear field theory," *Proceedings of the Royal Society of London. Series A. Mathematical and Physical Sciences* **260**(1300), 127–138 (1961).

[3] Vollhardt, D. and Wolfle, P., [*The Superfluid Phases of Helium 3*], Dover Books on Physics, Dover Publications (2013).

[4] Rho, M. and Zahed, I., [*The Multifaceted Skyrmion*], WORLD SCIENTIFIC (2015).

[5] Sutcliffe, P., "Skyrmions, instantons and holography," *Journal of High Energy Physics* **2010**(8) (2010).

[6] Al Khawaja, U. and Stoof, H., "Skyrmions in a ferromagnetic Bose–Einstein condensate," *Nature* **411**, 918–920 (2001).

[7] Parmee, C. D., Dennis, M. R., and Ruostekoski, J., "Optical excitations of skyrmions, knotted solitons, and defects in atoms," *Communications Physics* **5**(1) (2022).

[8] Bogdanov, A. N. and Panagopoulos, C., "Physical foundations and basic properties of magnetic skyrmions," *Nature Reviews Physics* **2**(9), 492–498 (2020).

[9] Tokura, Y. and Kanazawa, N., "Skyrmions in a ferromagnetic Bose–Einstein condensate," *Chemical Reviews* **5**(121), 2857–2897 (2021).

[10] Back, C., Cros, V., Ebert, H., Everschor-Sitte, K., Fert, A., Garst, M., Ma, T., Mankovsky, S., Monchesky, T. L., Mostovoy, M., Nagaosa, N., Parkin, S. S. P., Pfleiderer, C., Reyren, N., Rosch, A., Taguchi, Y., Tokura, Y., von Bergmann, K., and Zang, J., "The 2020 skyrmionics roadmap," *Journal of Physics D: Applied Physics* **53**(36), 363001 (2020).

[11] Tsesses, S., Ostrovsky, E., Cohen, K., Gjonaj, B., Lindner, N. H., and Bartal, G., "Optical skyrmion lattice in evanescent electromagnetic fields," **361**(6406), 993–996 (2018).

[12] Gao, S., Speirits, F. C., Castellucci, F., Franke-Arnold, S., Barnett, S. M., and Götte, J. B., "Paraxial skyrmionic beams," *Physical Review A* **102**(5) (2020).

[13] Sugic, D., Droop, R., Otte, E., Ehrmanntraut, D., Nori, F., Ruostekoski, J., Denz, C., and Dennis, M. R., "Particle-like topologies in light," *Nature Communications* **12**(1) (2021).

[14] Gutiérrez-Cuevas, R. and Pisanty, E., "Optical polarization skyrmionic fields in free space," *Journal of Optics* **23**(2), 024004 (2021).

[15] Forbes, A., de Oliveira, M., and Dennis, M. R., "Structured light," *Nature Photonics* **15**(4), 253–262 (2021).

[16] Rosales-Guzmán, C., Ndagano, B., and Forbes, A., "A review of complex vector light fields and their applications," *Journal of Optics (United Kingdom)* **20**(12) (2018).

[17] Galvez, E. J., Khadka, S., Schubert, W. H., and Nomoto, S., "Poincaré-beam patterns produced by nonseparable superpositions of laguerre–gauss and polarization modes of light," *Appl. Opt.* **51**(15), 2925–2934 (2012).

[18] Cisowski, C., Franke-Arnold, S., and Ross, C., "Building ideal paraxial optical skyrmions using rational maps," **2200350** (2022).

[19] Barnett, S. M., Franke-Arnold, S., Götte, J. B., McWilliam, A., Speirits, F. C., Ye, Z., and Cisowski, C. M., "Theory of paraxial optical Skyrmions." To be published.

[20] Zhu, J., Liu, S., and Zhang, Y.-S., "Synthesis and observation of optical skyrmionic structure in free space." arXiv:2103.11293v2 [quant-ph] (2021).

[21] Shen, Y., Martínez, E. C., and Rosales-Guzmán, C., "Generation of Optical Skyrmions with Tunable Topological Textures," *ACS Photonics* (2022).

[22] Bekshaev, A. Y., Soskin, M. S., and Vasnetsov, M. V., "An optical vortex as a rotating body: Mechanical features of a singular light beam," *Journal of Optics A: Pure and Applied Optics* **6**(5) (2004).

[23] Arora, G., Joshi, S., Singh, H., Haridas, V., and Senthilkumaran, P., "Perturbation of V-point polarization singular vector beams," *Optics and Laser Technology* **158**(PA), 108842 (2023).

[24] Geng, Y., Hu, H., Ma, X., Hu, X., Chai, X., Wang, X., Xi, S., and Zhu, Z., "Generation and characteristics of hollow structured optical fields based on multiple off-axis vortices," *Opt. Express* **31**, 27407–27419 (Aug 2023).

[25] Fösel, T., Peano, V., and Marquardt, F., "L lines, C points and Chern numbers: Understanding band structure topology using polarization fields," *New Journal of Physics* **19**(11) (2017).

[26] Siegman, A. E., [*Lasers*], University Science Books (1986).

[27] Selyem, A., Rosales-Guzmán, C., Croke, S., Forbes, A., and Franke-Arnold, S., "Basis-independent tomography and nonseparability witnesses of pure complex vectorial light fields by Stokes projections," *Physical Review A* **100**(6), 063842 (2019).

[28] Rosales-Guzmán, C., Hu, X. B., Selyem, A., Moreno-Acosta, P., Franke-Arnold, S., Ramos-Garcia, R., and Forbes, A., "Polarisation-insensitive generation of complex vector modes from a digital micromirror device," *Scientific Reports* **10**(1), 1–9 (2020).

[29] Shen, Y., "Topological bimeronic beams," *Optics Letters* **46**(15), 3737 (2021).

[30] Barnett, S. M., Speirits, F. C., and Götte, J. B., "On lines of constant polarisation in structured light beams," *Epl* **143**(3) (2023).

[31] Teng, H., Zhong, J., Chen, J., Lei, X., and Zhan, Q., "Physical conversion and superposition of optical skyrmion topologies," *Photon. Res.* **11**, 2042–2053 (Dec 2023).

[32] Singh, K., Ornelas, P., Dudley, A., and Forbes, A., "Synthetic spin dynamics with bessel-gaussian optical skyrmions," *Opt. Express* **31**(10), 15289–15300 (2023).